Proceedings of the Fifth International Symposium
on
Advanced Nuclear Energy Research
NEUTRONS AS MICROSCOPIC PROBES

I–9

POLYMER RESEARCH BY NEUTRON SCATTERING

D. Richter

Institut für Festkörperforschung
Forschungszentrum Jülich
D–5170 Jülich, Germany

ABSTRACT

Polymer physics aims on an understanding of the macroscopic behavior of polymer systems on the basis of their molecular structure and dynamics. For this purpose neutrons serve as a unique probe, allowing a simultaneous investigation of polymer structure and dynamics on a molecular scale. Furthermore, hydrogen deuterium exchange facilitates molecular labeling and offers the possibility to observe selected chains or chain parts in dense systems. Neutron small angle scattering reveals information on the conformation and possible aggregation of polymer chains. Data on linear and star like molecules are shown as examples. High resolution neutron spin–echo spectroscopy observes the molecular dynamics of long chain molecules. Results on the large scale motion of chains in polymer melts are presented. Finally, experiments on chain relaxation close to the glass transition are displayed. Three distinctly different relaxation processes are revealed.

INTRODUCTION

Macroscopic properties of polymeric matter like the mechanical behavior: the moduli, the strength, the viscoelasticity or transport properties and phase behavior are considered to be understood, if they are explained on the basis of molecular structure and dynamics. In order to fulfill this task, subtle probes are needed which are sensitive to the relevant molecular space and time regimes. Most important are scattering methods like X–ray and neutron scattering. Photons cover an extremely broad wavelength spectrum and are used both for structural and dynamic investigations. Unfortunately, however, the achievable time resolution which is associated with the photon energy and the spatial resolution, related to the wavelength, do not correspond. Thermal and cold neutrons, on the other hand, offer wavelengths in the molecular range and, at the same time, energies in the thermal region. This makes them a unique probe, allowing a simultaneous space–time observation of atomistic and molecular processes. Secondly, due to the nature of the scattering process occuring at the nuclei, isotop exchange facilitates atomistic labeling without strongly disturbing the chemical nature of the molecules. In particular, the different scattering properties of hydrogen and deuterium allow contrasting of organic substances. For example, only neutron scattering could access such basic properties as the chain dimension of a polymer in the bulk state.

STRUCTURAL INVESTIGATIONS

Medium and large scale structures are accessed by small neutron scattering (SANS). SANS machines are built on the principle of a pin hole camera. Neutron monochromatization is performed by a velocity selector. Thereafter, a collimation section prepares the appropriate divergence of the incoming beam. The scattered neutrons are counted with a multi detector, positioned in a flight tube at a variable distance from the sample. In this way, momentum transfers, down to about 10^{-3} Å^{-1} are reached, covering a spatial range up to several thousand Å. The Bonse–Hardt camera, using the intrinsic width of Bragg reflections from perfect silicon crystals as resolution elements, extends this observation window into the range of microns. SANS today is one of the most wide spread applications of neutron scattering. In the following two recent examples are given.

Temperature dependent chain dimension in polymer melts

Already the first SANS applications to polymer physics aimed on the evaluation of the polymer conformation in a melt /1/. Thus, it may be amazing that still substantial results may be obtained. Neutron scattering on a labeled chain in a polymer melt reveals the chain form factor, containing the chain conformation and, in particular, the chain dimension

$$R_g^2 = \frac{1}{6} C_\infty(T) \ell^2 N \qquad (1)$$

where R_g is the radius of gyration, C_∞ the characteristic ratio, ℓ the main chain bond length and N the number of bonds along the chain. The most important and generally accepted model for the evaluation of polymer conformations, the rotational isomeric state model (RIS) by Flory /2/, calculates the chain conformation in the ideal state on the basis of local interactions between rotational isomers of different bonded states. Non bonded interactions are taken into account only locally. The characteristic ratio, C_∞, is thus only related to local interactions along the chain. The population of rotational isomeric states depends on temperature via the balance between entropy and energy. In general, with increasing temperature, a chain will shrink because more gauche states are occupied, allowing the chain to coil more. A precise measurement of the temperature dependence of R_g, and thus of C_∞ (T) allows a detailed experimental access to this mechanisms.

Figure 1 presents SANS data from poly(ethylene–propylene) alternating copolymer (PEP), taken at different temperatures in form of a Zimm plot /3/. The Zimm plot takes advantage of the low Q expansion of the scattering function

$$\frac{1}{S(Q)} = \frac{1}{\phi(1-\phi)V_w}\left(1+\frac{Q^2R_g^2}{3}\right) \qquad (2)$$

where S(Q) is the absolutely normalized scattering intensity, ϕ the polymer concentration, V_w the scattering volume. The decreasing slopes of the scattering curves in Figure 1 thus indicate the gradual reduction of the radius of gyration with increasing temperature. The upper part of Figure 2 displays the resulting temperature dependence of R_g for PEP /3/. Within the observation window, R_g decreases by about 10 %, exhibiting a temperature coefficient $\kappa = -1.16 \cdot 10^{-3}$ K^{-1} in close agreement with the prediction of the RIS model ($\kappa = -1.1 \cdot 10^{-3}$ K^{-1}) and earlier results on Θ solvents ($\kappa = 1 \cdot 10^{-3}$K^{-1}). As a new feature, the SANS data reveal a gradual decrease of κ with increasing

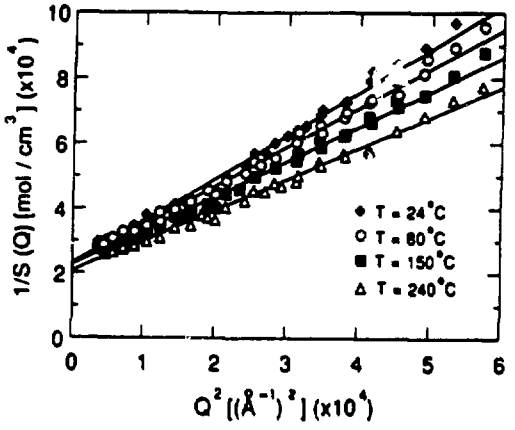

Fig.1: Zimm plot of the SANS data from the PEP sample at various temperatures.

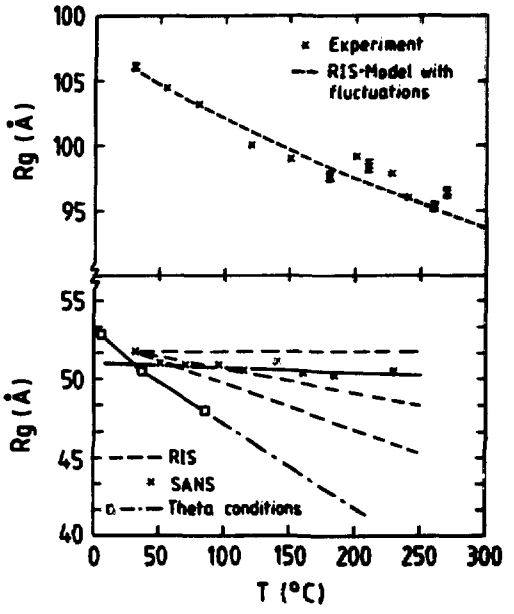

Fig.2: Experimental and theoretical results for the temperature dependence of the radius of gyration for polyethylene–propylene (a) and polypropylene (b). The dashed lines give predictions of the RIS model.

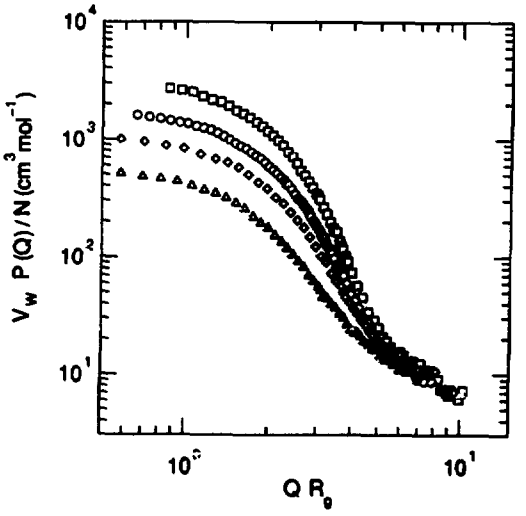

Fig.3: Form factors for monodisperse polymer stars with functionalities between 8 and 64 (from below). The radius of gyration were obtained from the maximum in the Kratky plot.

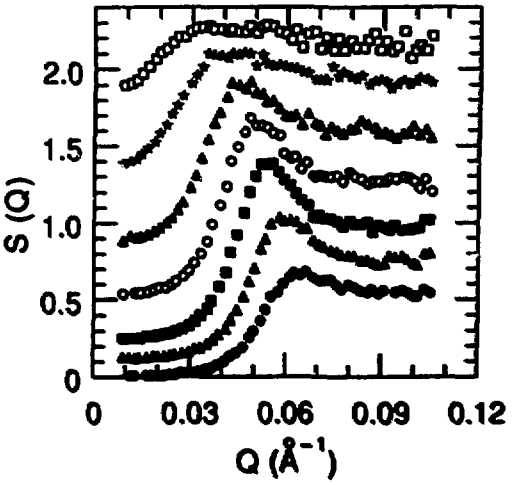

Fig.4: Structure factors for 18 arm stars solutions for some representative concentrations (• 19.2%; ▲ 14.6%; ▪9.9%; o 7.4%; ▵ 2.5%; * 1.5%; □ 1 %) For a better visualization the data are offset by an additive constant.

temperature. We emphasize the excellent quantitative agreement between RIS predictions and experimental results. Compared to earlier experiments using different Θ solvents, SANS on polymer melts has the advantage of a much larger temperature range, combined with the absence of specific solvent effects.

With this result and a similar experiment on polyethylene /4/ at hand, one could be satisfied and take the RIS model finally for granted. However, further experiments on polymers with higher side group density (polypropylene, (PP)) or larger side groups (polyethylethylene, (PEE)) led to a pronounced disagreement with RIS predictions, which apparently cannot be reconciled /5/. As an example, the lower part of figure 2 presents the temperature dependent radius of gyration for atactic PP. As for isotactic PP /6/, the radius of gyration is practically independent of temperature. This result contrasts to Θ solvent data and disagrees to most of the RIS predictions. In particular, the independence on tacticity cannot be explained in terms of a RIS ansatz. Similar discrepancies are found for PEE. Obviously, more numerous or larger side groups cause severe difficulties for a description of C_m in terms of very local interactions, which is the basis of RIS.

Star polymers in solution

Star polymers consist of linear chains, connected at one central point and can be considered as prototype materials for branched polymers. They also have practical interest, for example, as viscosity modifiers in motor oils. Their conformation is described in analogy to semidilute polymer solution as a succession of spatially inhomogeneous blobs, growing from the center to the rim /7/. Progress in the technique of anionic polymerization allows the synthesis of monodisperse stars with functionalities up to f = 128. Figure 3 presents the forms factors of a series of stars with different functionalities ($8 < f < 64$) /8/. The scattering curves have been normalized to the monomer concentration. The Q scale was adjusted to the radius of gyration. While in the tails the scattering curves from all stars collapse to a single curve – here we observe the scattering from single arms, which is identical for all stars – at low Q with increasing functionality an increasingly important build–up of intensity is observed. This intensity increase originates from the coherent superposition of intensity from the different arms and, accordingly, is proportional to f.

Star polymers in dilute solution represent a very inhomogeneous monomer density distribution. Increasing the monomer concentration, therefore, leads to an important osmotic repulsion between different stars. Other than linear chains, which interpenetrate easily, star polymers exhibit ordering phenomena in the neighborhood of the overlap concentration Φ^*. Varying concentration and functionality, such ordering phenomena were investigated systematically on a series of stars /8,9/. The interstar structure factor S(Q) was evaluated on the basis of

$$S(Q) = I(Q)/(\Phi V_w P_0(Q)) \qquad (3)$$

Thereby, I(Q) is the normalized intensity and P(Q) is the polymer form factor, which was taken from the low concentration extrapolation of the intensity. The thus obtained structure factors for an 18 arm polyisoprene star solution are shown in figure 4. From low to high concentration, we observe the gradual development of a peak structure which is maximal around $\Phi \approx 10$ % and diminishes towards higher concentration. (With $\Phi^* = V_w/(4/3\pi Rg^3)$ we arrive at 10.1 %). We note that S(Q) at high Q does not reach unity but levels off towards lower values. Most likely this is caused by a form factor, changing with concentration, which is not considered in equation 3. Figure 4 also shows that the position of the maximum in S(Q) increases with increasing concentration.

Comparing stars and linear polymers, in dilute solution the osmotic pressure in both cases is proportional to the number of molecules in solution. In the semidilute regime, where the branches of different stars or linear polymers, respectively, interpenetrate, we have a more or less uniform segment distribution. There, the osmotic pressure is given by the number of blobs in the system. $\Pi \approx kT\ \xi(\Phi)^{-3}$, where $\xi(\Phi)$ is the blob size. Around Φ^*, a transformation occurs from a state where, with respect to the osmotic pressure, all arms of one star act as one entity to another state where each arm does not know anymore to which star it belongs and acts separately. As a consequence, a sudden increase of the osmotic pressure is required. This extra osmotic pressure is the basis of the repulsion between polymer stars. Witten et al /10/ have worked out a scaling theory and predict that a jump in the osmotic pressure should be proportional to $f^{3/2}$. Accordingly, also the peak height in S(Q) should follow $f^{3/2}$ scaling.

Figure 5 displays the structure factor S(Q) for the different stars at the overlap concentration Φ^*. In order to make them comparable, the structure factors were scaled such that in the high Q limit all S(Q) curves approach 1. Figure 5 demonstrates the build–up of structure in going to higher functionality. While for the f = 8 arm star, the peaks in the structure factor is barely developed, with increasing functionality the peak sharpens up and narrows. The insert in figure 5 displays the relative peak height $S(Q_{max})/S(0)$ as a function of functionality. The solid line displays the predicted $f^{3/2}$ behavior. Within experimental accuracy, the results at the lower functionalities follow the theoretical prediction well while the peak height for the 64 arm star is clearly larger, possibly an indication for macrocrystalline ordering. The formation of a macrocrystal at f = 64 is further evidenced by the observed two dimensional intensity pattern. There, the peak shows itself in form of a concentric ring around the Q = 0 position. For a liquid, the intensity distribution along the ring should be homogeneous. In the case of the 64 arm star, bright spots at certain positions along the ring indicate preferred orientations or a grain structure in the sample which cannot possibly be caused by a liquid like state. Further experiments will be necessary to get to the details of the macrocrystalline order.

DYNAMIC EXPERIMENTS

The interesting mechanical dynamical properties of polymer systems relate to the large scale motions of polymer chains. Observation of their space time evolution requires extremely high resolution neutron spectroscopy, operating at low angles. Neutron spin–echo spectroscopy (NSE) is well adapted to this task. Decoupling energy resolution and intensity, neutron spin–echo directly measures velocity differences of incoming and scattered neutrons in comparing the number of Larmor precessions of the neutron spin in magnetic guide fields before and after scattering. In this way, relative energy resolutions in the order of 10^{-5} may be achieved with an incoming wave length band of 20 % width. Presently, neutron spin–echo experiments are only available at the ILL in Grenoble and at the LLB in Saclay. Further neutron spin–echo spectrometers are being built in Germany and Japan. While NSE is the basic instrument for the investigation of polymer dynamics, time of flight methods are also of interest in order to reveal faster relaxation processes and soft phonons, which are in particular important in relation to the glassy behavior of polymer systems.

Molecular dynamics in a polymer melt – direct observation of entanglement distances

High molecular weight polymeric liquids exhibit unusual dynamic properties. Depending on the time scale of observation or temperature, the same polymer may

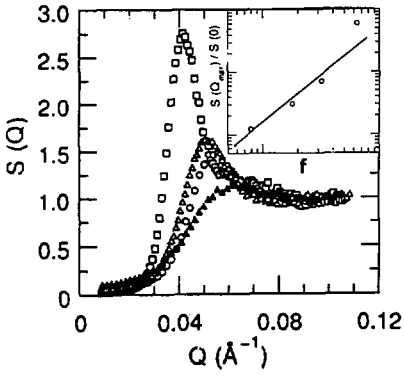

Fig.5: Structure factors S(Q) for stars with the functionalities f = 8 ▲; f = 18 o; f = 32 Δ; and f = 64 □. The structure factors are taken at the overlap concentration Φ^*. The insert displays the ratio $S(Q_{max})/S(0)$ as a function of functionality.

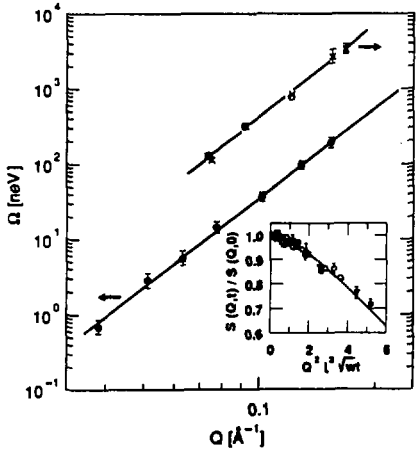

Fig.6: Characteristic frequency for the Rouse decay for different polyisoprene samples as a function of Q. The insert displays the scaling behavior of the dynamic structure factor if plotted versus the Rouse scaling variable $Q^2 \cdot \ell^2 \cdot \sqrt{Wt}$. the different symbols correspond to different Q values. (The scale on the right side is offset by a factor of ten.)

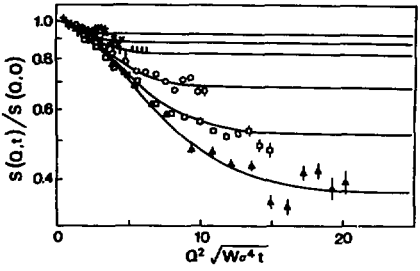

Fig.7: Dynamic structure factor from PEP, displayed in a scaling plot against the Rouse variable. Q values from above (0.058 Å^{-1}; 0.068 Å^{-1}; 0.078 Å^{-1}; 0.097 Å^{-1}; 0.117 Å^{-1}; 0.135 Å^{-1}). The solid lines are the result of a fit with the Ronca model.

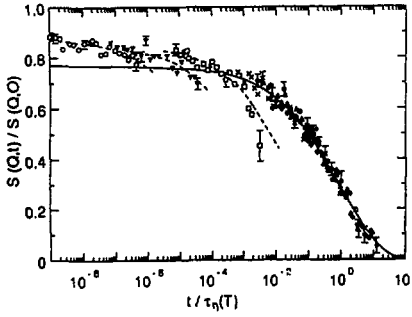

Fig.8: Neutron spin–echo result from polybutadiene approaching the glass transition. The data are scaled with the viscosity time scale τ_η. The solid line represents the master function obtained for the spectra at temperatures ≥ 220 K. The dashed lines are the result of fitting stretched exponentials to the different low T spectra, keeping $\beta = 0.37$ fixed. ♦ 280 K; • 260 K; ▲ 250 K; ◇ 240 K; x 230 K; □ 205 K; ▼ 190 K; o 180 K.

respond elastically, showing rubber like behavior or may flow like a liquid. This ambiguity in its mechanical properties is also also termed viscoelastic. The rubbery behavior which expresses itself by the the so–called plateau regime in the dynamic modulus, is commonly attributed to the effect of entanglements. They are thought to stem from geometrical or topological constraints, mutually imposed by the interpenetrating chain molecules. Their molecular origin, however, is not well understood. The reptation theory of viscoelasticity /11/ bases on the further assumption that the geometrical constraints can be modeled by a tube confinement, surrounding a given chain. At intermediate times, the polymer dynamics are restricted to a curve linear motion along the tube. The tube diameter d, thereby, may be interpreted as a distance between entanglements.

If chains could intersect freely, the chain dynamics would be described as thermal motion, damped via a friction coefficient ζ. In this so–called Rouse model/11/, the diffusing chain segments perform a random walk on the random chain profile. This convolution of two random processes leads to a mean square segment displacement $\langle r^2(t)\rangle \approx \ell^2/Wt$ with $W = 3kT/\zeta\ell^2$, being the Rouse rate. In Gaussian approximation, the dynamical correlation functions relate directly to the mean square segment displacement and scale with the universal Rouse variable $u = Q^2/W\ell^4 t$. Their characteristic frequency depends on the fourth power of the momentum transfer.

The presence of an intermediate dynamic length scale, d, changes the scaling behavior of S(Q,t) and causes systematic Q dependent deviations from the Rouse scaling. In the frame work of reptation, de Gennes derived an explicit first order expression for S(Q,t) /12/

$$S(Q,t)/S(Q) = 1 - \frac{Q^2d^2}{36} + \frac{Q^2d^2}{36}\exp\left(\frac{u^2}{36}\right)\operatorname{erfc}\left(\frac{u}{6}\right) \qquad (4)$$

The important feature in equation 4 is the factor $Q \cdot d$, which introduces the new length scale. Due to the tube constraints, S(Q,t), only partially decays to a certain Q dependent fraction. The remaining elastic part is a consequence of long living segment–segment correlations due to the tube confinement. This elastic part actually decays only for times longer than a terminal time, τ_d, after which the chain has lost its memory of the original tube. At short times, when a polymer segment does not yet realize the spatial constraint, Rouse behavior should prevail. Figure 6 displays characteristic frequencies, derived from the initial decay of NSE spectra obtained from polyisoprene melts at 200° C /13/. The solid lines represent the $\Omega \propto Q^4$ law. A similar result has recently been reported for PDMS /14/, where geometrical constraints are supposed to be even less pronounced than for polyisoprene. The insert in figure 6 demonstrates the scaling behavior of the experimental spectra which, according to the Rouse model, are required to collapse to one master curve if they are plotted in terms of the Rouse variable u. The solid line displays the result of a joint fit to the Rouse structure factor, the only fit parameter being the Rouse rate. An excellent agreement with theoretical prediction is observed.

The effect of entanglement constraints on polymer dynamics in polymer melts has been investigated on polyethylene (PEB), polyethylene propylene (PEP) and polyisoprene (PI) /13,15,16/. The results for all polymers are displayed in table 1. Here we remark only on the data from PEP. Figure 7 presents the measured dynamic structure factor for PEP at 492 K in a scaling form. The data are characterized by common initial decay, signifying the Rouse regime and a consecutive Q dependent cross–over into a plateau, resulting from the presence of an intermediate dynamic length scale beyond which density fluctuations are strongly limited. The solid line represents the result of a fit with a model by Ronca /17/, dealing with the cross–over from Rouse to entanglement controlled dynamics. It allows a very satisfying description of the experimental data, reproducing the line shape, the resulting sharp cross–over, and the Q dependence

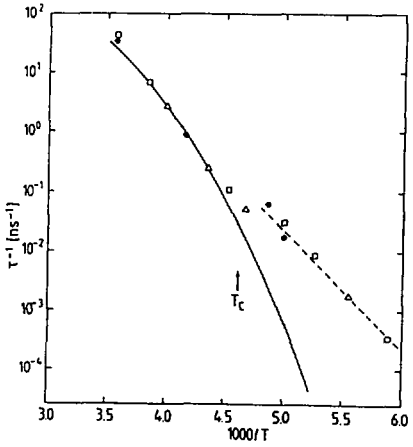

Fig.9: Arrhenius representation of the relaxation rate obtained from fitting stretched exponentials to the spectra from polybutadiene at different temperatures. The solid line displays the viscosity time scale. The dashed line indicates the Arrhenius behavior of the low temperature branch.

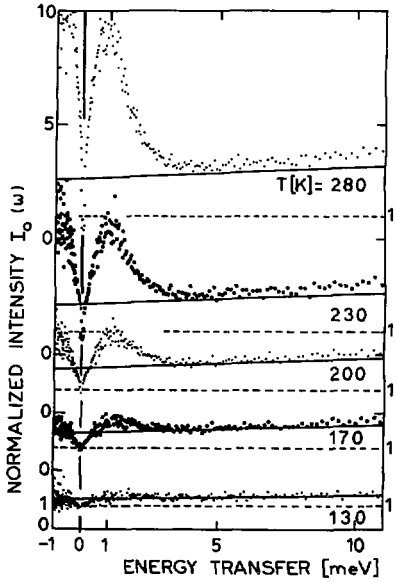

Fig.10: Temperature dependence of normalized intensities for polybutadiene as a function of energy transfers as measured with time of flight spectroscopy. The elastic intensity has been subtracted. The spectra are normalized to T = 100 K. The dashed line gives the reference value 1 — no intensity change. The solid line is a calculation of the expected intensity increase, resulting from the Bose–Einstein occupation factor and the extrapolated low temperature Debye–Waller factor. The width of the vertical line marks the instrumental elastic resolution.

Table 1: NSE results on polymer melts

		NSE			Rheology	
Sample	T[K]	d[Å]	$10^9\zeta[\frac{dyns}{cm}]$	τ_e[ns]	d[Å]	$10^9\zeta[\frac{dyns}{cm}]$
PI 1	468		4.4±0.3	-		
PI 2	473	52±1	3.8±0.3	32	51(298K)	
PEP homopolymer	492	47.5±0.4	3.1±0.1	15	43.5±2	1.9
PEP triblock	491	47.1±0.7	2.4±0.2	15		
PEB-2	509	43.5±0.7	0.4±0.04	5	35(373K)	0.3(448K)[†]

of the plateau levels. In order to compare with rheology, rheological data for the plateau modulus were converted into tube diameters using the reptation model /11/. They are included in table 1. In all cases the microscopically determined entanglement distances agree well with those obtained from rheology using the reptation concept.

Polymer motion near the glass transition

While the previous section dealt with large scale motion, here we are interested in the very local dynamics, i.e., the elementary motional processes. I present data on cis–trans–vinyl (46:47:7)polybutadiene (PB), $(CD_2CD{=}C\bar{D}CD_2)_n$. This polymer consists essentially of a backbone only. The randomness of the chain structure is related to the random distribution of the two stable C bond orientations (cis and trans) relative to the double bond. Diffraction experiments reveal a static structure factor with a first peak due to interchain correlations around $Q = 1.5$ Å^{-1}, followed by a minimum around 2 Å^{-1}.

Figure 8 displays a set of NSE spectra, taken close to the first minimum of the structure factor /18/. The NSE spectra reveal a strongly stretched exponential relaxation $\exp-(t/\tau)^{\beta}$ with β - 0.4. Spectra taken at different temperatures have been rescaled on the basis of the time scale, $\tau\eta$, set by the viscosity. At temperatures above 220 K, all experimental data collapse to a single master curve. At lower temperatures the rescaled spectra depart distinctly from such a behavior. Thus, above 220 K the dynamics at the level of interchain distances scale directly with the time scale, set by macroscopic viscosity. The freezing of all polymer relaxation modes from the slowest mode which dominates viscosity, to the fastest modes which are observed in the spin–echo experiments, follow the same time scale $\tau\eta$. This result is by no means trivial and recently has become the subject of theoretical debate. Thus, above 220 K, NSE observes the structural relaxation or α relaxation, which completely dominates the dynamics. We note that the amplitude or spectral contribution of this relaxational process appearently stays constant. The master curve for all relaxation spectra extrapolates to 0.77 for $t \rightarrow 0$. Consequently, an important part of the spectrum decays outside the observation window of the spin–echo spectrometer.

Below 220 K the microscopic relaxation does not slow down as much as the viscosity. A single universal time scale for all length scales is no longer valid. We note that also the spectral contribution of the observed relaxation process starts to increase below 220 K. Figure 9 displays the observed relaxation rates in term of an Arrhenius diagram. The solid line, thereby, represents the temperature dependent viscosity time scale $\tau\eta$. While above 220 K the good agreement between microscopic rates and $\tau\eta$ is evident, below 220 K a strong decoupling of both scales is obvious. The relaxational process observed at low temperature reveals strong similarities to β relaxation processes as observed with dielectric spectroscopy in other materials.

We now turn to the question of the missing intensity in the NSE spectra, indicating a second relaxation step at higher frequency. Figure 10 /19/ displays the results of time of flight experiments where the elastic scattering contribution was subtracted. At large energy transfers ($E > 3$ meV), the experiment observes harmonic phonons obeying Bose statistics (solid lines). Additional intensity is observed around 2 meV which increases strongly for temperatures above T_g. This intensity is the spectral contribution giving rise to the gap in the NSE spectra and constitutes a third fast relaxational process which seems to be characteristic for glass forming systems and has been observed in glass formers as different as ionic glasses, molecular glasses and polymers. These fast relaxation processes may be related to the soft phonon modes, which appear to be characteristic for the glassy state.

In summary, approaching the glass transition, the main chain polymer polybutadiene exhibits three distinctly different relaxation processes. (i) The structural or α

relaxation dominates above 220 K all relaxation processes from viscosity to microscopic relaxation. (ii) Below 220 K the microscopic relaxation decouples from the viscosity time scale. At this temperature the spectral contribution of the microscopic relaxation shows a cusp–like behavior /20/. In a polymer without side groups this relaxation must relate to main chain motions and may be understood as a frustrated α relaxation which does not contribute anymore to macroscopic flow. (iii) In addition, a fast relaxational process is observed which is characterized by nearly constant relaxation rate and a rapidly increasing intensity above T_g.

RESUME

Neutron scattering has proven to be a unique probe for the investigation of soft matter in particular polymers. This is mainly due to the possibility of contrast variation by hydrogen–deuterium exchange and the capability of a simultaneous investigation in space and time. For structural investigation with medium resolution, neutron small angle scattering today is the standard method governing the field. Access to the relevant large scale slow dynamic processes is obtained by neutron spin–echo spectroscopy. Other than in the case of SANS where ample possibilities exist worldwide, the NSE method still has to spread in order to cover the demand.

REFERENCES

/1/ R.G. Kirste, W.A. Kruse, J. Schelten Die makromolekulare Chemie **162**, 299 (1973)
/2/ P.J. Flory Statistical Mechanics of Chain Molecules, Wiley, New York (1969)
/3/ A. Zirkel, D. Richter, W. Pyckhout–Hintzen, L.J. Fetters Macromolecules **25**, 954 (1992)
/4/ A.T. Boothroyd, A.R. Rennie, C.B. Boothroyd Europhysics Lett. **15**, 715 (1991)
/5/ A. Zirkel, V. Urban, D. Richter, L.J. Fetters, J.S. Huang, R. Kampmann, N. Hadjichristidis Macromolecules **25**, 6148 (1992)
/6/ D.G. Ballard, P. Cheshire, G.W. Longman, J. Schelten Polymer **19**, 379 (1978)
/7/ M. Daoud, J.P. Cotton J. Phys. (Paris) **43**, 531 (1982)
/8/ D. Richter, O. Jucknischke, L. Willner, L.J. Fetters, M. Lin, J.S. Huang, J. Roovers, P. Toporowski, L.L. Zhou ACS Polymer Preprint Summer 1992
/9/ L. Willner, O. Jucknischke, D. Richter, B. Farago, L.J. Fetters, J.S. Huang Europhysics Lett. **19**, 297 (1992)
/10/ T.A. Witten, P.A. Pincus. M.E. Cates Europhysics Lett. **2**, 137 (1986)
/11/ M. Doi, S.F. Edwards The Theory of Polymer Dynamics, Clarend.Oxford (1986)
/12/ P.G. de Gennes J. Phys. (Paris) **42**, 735 (1981)
/13/ D. Richter, R. Butera, L.J. Fetters, J.S. Huang, B. Farago, B. Ewen Macromolecules **25**, 6156 (1992)
/14/ D. Richter, B. Ewen, B. Farago, T. Wagner Phys.Rev.Lett. **62**, 2140 (1989)
/15/ D. Richter, B. Farago, L.J. Fetters, J.S. Huang, B. Ewen, C. Lartigue Phys.Rev.Lett. **64**, 1389 (1990)
/16/ R. Butera, L.J. Fetters, J.S. Huang, D. Richter, W. Pyckhout–Hintzen, A. Zirkel, B. Farago, B. Ewen Phys.Rev.Lett. **66**, 2088 (1991)
/17/ G. Ronca J.Chem.Phys. **79**, 1031 (1983)
/18/ D. Richter, R. Zorn, B. Farago, B. Frick, L.J. Fetters Phys.Rev.Lett **68**, 1620 (1992)
/19/ B. Frick, D. Richter, W. Petry, U. Buchenau, Z. Physik **B70**, 73 (1987)
/20/ B. Frick, B. Farago, D. Richter, Phys.Rev.Lett. **64**, 2921 (1990)